Oxygen Vacancies on Layered Niobic Acid Weaken the Catalytic Conversion of Polysulfides in Lithium Sulfur Battery

Lingling Xu,[⊥][a] Hongyang Zhao,[⊥][a] Mingzi Sun,[⊥][c] Bolong Huang,*[c] Jianwei Wang,[a] Jiale Xia,[a] Na Li,[a] Dandan Yin,[a] Meng Luo,[a] Feng Luo,[d] Yaping Du,*[b] and Chunhua Yan[b,e,f]

Dedicated to 100th Anniversary of Nankai University

Abstract: Oxygen vacancies are usually considered as beneficial in catalytic conversion of polysulfides in lithium-sulfur batteries. In this work, we demonstrated that the conversion of polysulfides was hindered by oxygen vacancies on ultrathin niobic acid. The inferior performance induced by the oxygen vacancy was mainly attributed to the decreased electric conductivity as well as the weakened adsorption of polysulfides on the catalyst surface. This work showed that the care should be taken when designing a new catalyst for the lithium-sulfur battery using defect-engineering strategy.

Introduction

The increasing need for better electrically powered devices persuaded researchers to develop energy storage devices with higher energy density. Lithium-sulfur (Li-S) battery, expected to reach the energy density of 2600 Wh kg^{-1}, emerged as the most promising and practical candidate for future energy storage.[1] One of the most detrimental issues in Li-S batteries is the shuttle effect, which stems from the diffusion of polysulfides through the separator and depositing them on the lithium anode. The shuttle effect not only deactivates the lithium metal, but also results in loss of sulfur, and eventually leads to poor Coulombic efficiency and battery failure. In order to inhibit the shuttle effect, efforts have been made including atomic engineering of sulfur as well as kinetics optimization.[1b, 2] One of the most intensive investigated topics in Li-S battery kinetics is to study the catalytic conversion of polysulfides.

As a catalytic process, the adsorption of polysulfides is extremely important because it has one of the highest energy barriers in the conversion.[3] Without strong binding with polysulfides species, it was sluggish to promote the kinetics in Li-S battery.[4] Polysulfides can be regarded as Lewis bases and soft bases due to the electron-rich nature and low electronegativity. Therefore, a solid acid could act as an absorbent of polysulfides. Much effort has been devoted to this aspect based on the above hypothesis.[5] It is well known that surface acidity of solids is closely related to the oxygen vacancy concentration. It is natural to consider that more oxygen vacancies would benefit the catalytic conversion of polysulfides. There are many reports on the beneficial effect of oxygen vacancy on polysulfide conversion.[6] However, it should be noted that the adsorption of polysulfide conversion is a complex process which is related to the electric conductivity and surface electronic state. The generation of oxygen vacancies usually leads to a significant change in the physical properties of the material. Herein, we demonstrated that the fully oxidized HNb_3O_8 (HNO) was more active in catalytic conversion of polysulfides conversion compared with HNb_3O_8 with high oxygen vacancy concentration (HNO-v). The results gave us a hint that oxygen vacancies are not universally effective in catalytic conversion of polysulfides.

The ultrathin structures are considered as excellent models to study the adsorption behavior of polysulfides.[7] They possess a large electroactive surface with sufficient active sites for promoting the catalytic reactions.[8] Therefore, it is promising to use ultrathin structure

[a] L. Xu, H. Zhao,J. Wang, J. Xia, N. Li, D. Yin, M. Luo
Frontier Institute of Science and Technology, Xi'an Jiaotong University, Xi'an, Shaanxi 710054, China
[b] Prof. Y. Du, Prof. C. Yan
School of Materials Science and Engineering & National Institute for Advanced Materials, Key Laboratory of Advanced Energy Materials Chemistry, Tianjin Key Lab for Rare Earth Materials and Applications, Centre for Rare Earth and Inorganic Functional Materials, Nankai University, Tianjin, 300350, China
E-mail: ypdu@nankai.edu.cn (Y. Du)
[c] M. Sun, Prof. B. Huang
Department of Applied Biology and Chemical Technology, The Hong Kong Polytechnic University, Hung Hom, Kowloon, Hong Kong SAR, P. R. China
E-mail: bhuang@polyu.edu.hk (B. Huang)
[d] Prof. F. Luo
IMDEA Nanoscience, Faraday 9, Ciudad Universitaria de Cantoblanco, 28049 Madrid, Spain
[e] Prof. C. Yan
Beijing National Laboratory for Molecular Sciences, State Key Laboratory of Rare Earth Materials Chemistry and Applications, PKU-HKU Joint Laboratory in Rare Earth Materials and Bioinorganic Chemistry, College of Chemistry and Molecular Engineering, Peking University, Beijing 100871, China
[f] Prof. C. Yan
College of Chemistry and Chemical Engineering, Lanzhou University, Lanzhou 730000, China
⊥ These authors contributed equally.

Supporting information for this article is given via a link at the end of the document.

to study the difference between the pristine surface and oxygen-vacancy-defects rich surfaces, which is more evident for us to gain an insightful understanding of the surface defect in catalytic reactions. In this work, we have carried out a Lewis solid acid HNO ultrathin nanobelt for Li-S battery.

Results and Discussion

The ultrathin structured HNO nanobelts were synthesized by proton-exchange from KNb_3O_8 nanobelts followed by mild chemical exfoliation as illustrated in Figure 1a. Figure S1 shows the X-ray diffraction (XRD) pattern and transmission electron microscopy (TEM) image of the KNb_3O_8. Oxygen deficient HNO-v nanobelts were obtained by annealing in reducing atmosphere. Afterwards, sulfur was loaded on both nanobelts via melt-diffusion and denoted as HNO@S.

Scanning electron microscopy (SEM) image Figure 1b shows that the as-prepared HNO nanobelts are at a similar micrometer-scale length as KNb_3O_8 except that the thickness is significantly reduced. TEM demonstrates the width of 200-300 nm (Figure 1c, d). The high-resolution TEM (HRTEM) image in Figure 1e shows a clear lattice distance of 0.36 nm corresponding to the (240) facet of the HNO. Selected area electron diffraction (SAED) pattern shows that the HNO nanobelts are polycrystalline. The thickness of the HNO is about 7 nm from the atomic force microscope (AFM) image in Figure 1f. Energy-dispersive spectroscopy (EDS) elemental mapping of sulfur loaded HNO shows the homogeneous distribution of S on the nanobelts in HNO@S (Figure 1g).

XRD patterns of the as-synthesized HNO nanobelts before and after exfoliation are presented in Figure S2a. HNO nanobelts obtained by exfoliation have weaker and broader (020) diffraction peaks compared with the original HNO, revealing a less periodic structure, which is also an indicator of ultrathin structures.[9] Raman spectra of HNO-v showed no significant change in peak positions while the peak intensity reduced due to lower crystallinity, which is in accordance with the XRD results (Figure S2b).

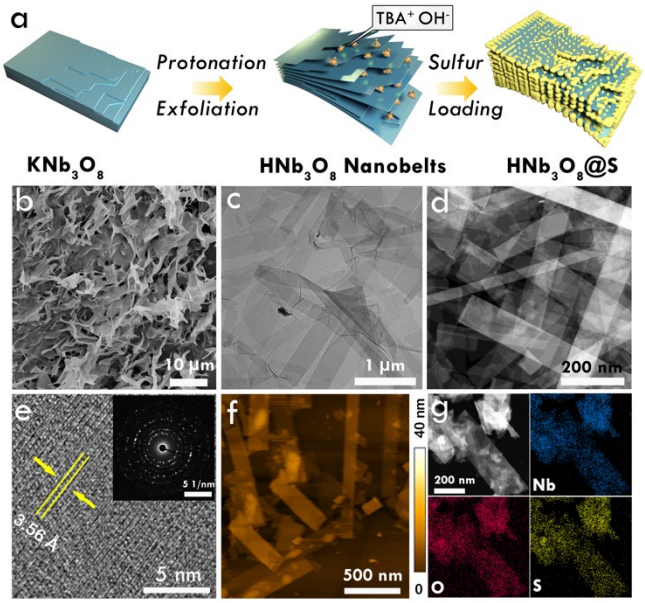

Figure 1. (a) Schematic illustration of the synthesis of the HNO@S. (b) SEM image and (c, d) TEM images of HNO nanobelts. (e) HRTEM image of HNO nanobelts. Inset: SAED pattern of HNO nanobelts. (f) AFM image of the HNO nanobelts. (g) Scanning TEM image of HNO@S and the corresponding EDS elemental mappings of Nb, O and S.

Electrochemical performance of both HNO@S and HNO-v@S are measured in coin cells. The sulfur content was about 68%, as confirmed by thermogravimetric analysis (TGA) (Figure S3). The tap density of the ultrathin HNO nanobelts was 0.53 g/cm^3. The pressed density of the HNO nanobelts and the HNO nanobelts loaded with sulfur were 2.81 and 2.26 g/cm^3 (Figure S4). The cross-sectional images of the electrodes and carbon nanotube interlayer were in Figure S5. As it can be seen from the cyclic voltammetry (CV) profiles (Figure S6a), the cathodic peaks at 2.32 and 2.02 V corresponded to the forming of lithium polysulfides (Li_2S_n, $4 \leq n \leq 8$) from S_8, and subsequently reduced to short-order Li_2S_2/Li_2S, which were denoted as Peak I and Peak II, respectively. The anodic peaks in the reverse scan located at 2.35 V with a shoulder peak at 2.41 V stem from the oxidation of Li_2S/Li_2S_2 to long-order Li_2S_n and then S_8, which were denoted as Peak III&IV. In comparison, the slight negative shift of the oxidation peak of HNO electrode indicates that HNO is more advantageous in facilitating the oxidation of short-order polysulfides to long-order polysulfides for better sulfur utilization.

We studied the redox kinetics of sulfur in both HNO and HNO-v catalysts by analyzing the CV curves. Due to electrode polarization, the anodic peaks shift to higher potentials while cathodic peaks shift to lower potentials with increasing scan rates. HNO electrode showed an obvious smaller polarization compared with the HNO-v electrode. Peak I, Peak II and Peak III&IV of HNO electrode shifted 0.05, 0.08, and 0.07 V with a scan rate increase from 0.2 to 2.0 mV s^{-1}; while for HNO-v electrode, Peak I, Peak II and Peak III&IV

shifted 0.05, 0.10, and 0.11 V, respectively (Figure 2a). The smaller polarization indicates that the HNO electrode is much more kinetically favorable than the HNO-v electrode. In comparison, CV curves of the pure sulfur cathode showed that the polarization is even serious (Figure S7a).

In order to further elucidate the kinetics difference of peaks in detail, we analyzed the relationship between scan rates and peak current, which obeys the following equation:[10]

$$i = av^b \quad (1)$$

Where i is the current value, v is the scan rate and b is an indicator of electrode kinetics between 0.5 and 1. Higher b-value indicates the redox reaction can proceed at high current densities, which implies a better rate performance. It can be seen from Figure 2b that the b-values of the HNO electrode are 0.96, 0.49 and 0.8 at the peak I, peak II and peak III&IV, respectively, while the corresponding b-values of HNO-v electrode are 0.74, 0.46 and 0.68 (Figure S6b-d). Given that peak I is the conversion of sulfur to Li_2S_4, and III&IV is Li_2S to sulfur, the catalytic activity of HNO outperformed HNO-v in both formation and conversion of polysulfides. The b-values of the sulfur cathode are much smaller than the HNO electrode, which indicates enhanced kinetics after introducing HNO in the electrode (Figure S7c-d). By carefully examining the onset potential values of the Peak I, II and III&IV, we can find that HNO showed a remarkably lower overpotential than HNO-v that further confirmed HNO was more kinetically favorable for polysulfide conversion (Figure 2c). Besides, the electrochemical impedance spectroscopy (EIS) test also reflected that the HNO electrode showed a lower charge-transfer resistance compared with the HNO-v and pure sulfur cathodes (Figure S8).

The catalytic activity of the electrode is playing a pivotal role in determining the performance of batteries at high current rates. Figure 2d shows the 20th galvanostatic discharge-charge curves of the HNO and HNO-v electrode at a high current rate of 5 C. The discharge capacities for the HNO and HNO-v electrodes are 680, 600 mAh/g, respectively. The plateau voltage gap (Δ) of the two electrodes is highly correlated to the electrode polarization. Notably, the voltage gap between second charge/discharge plateaus of HNO (ΔE = 182 mV) is much smaller than HNO-v (ΔE = 230 mV), indicating that better kinetics of HNO at high charge/discharge rate. This would naturally lead to much higher performance of HNO than HNO-v at high current rates.

The long-term cycle performance of the HNO, HNO-v, pure sulfur electrodes at a current density of 1C are shown in Figure S9. The HNO electrode delivers an initial capacity of 1081 mA h/g and 680 mA h/g maintained after 500 cycles with a capacity decay rate of 0.07% per cycle. The discharge capacity after 500 cycles of HNO-v electrode is 597 mA h/g, which is lower than the HNO. The HNO/HNO-v contribute negligible capacity of only xx (Supplementary Fig 10). Besides, CNTs interlayer can effectively improve the utilization efficiency of sulfur (Figure S11). To further demonstrate the stability and high capacity of HNO electrode at high rates, the cycle performance at 5C is shown in Figure 2e. The HNO electrode exhibits a capacity of 640 mA h/g after 250 cycles with excellent stability. As for HNO-v electrode, although the initial capacity is the same with HNO electrode, the capacity faded fast within 20 cycles. This indicated that the adsorption of polysulfides on HNO-v is less strong than on the HNO electrode.

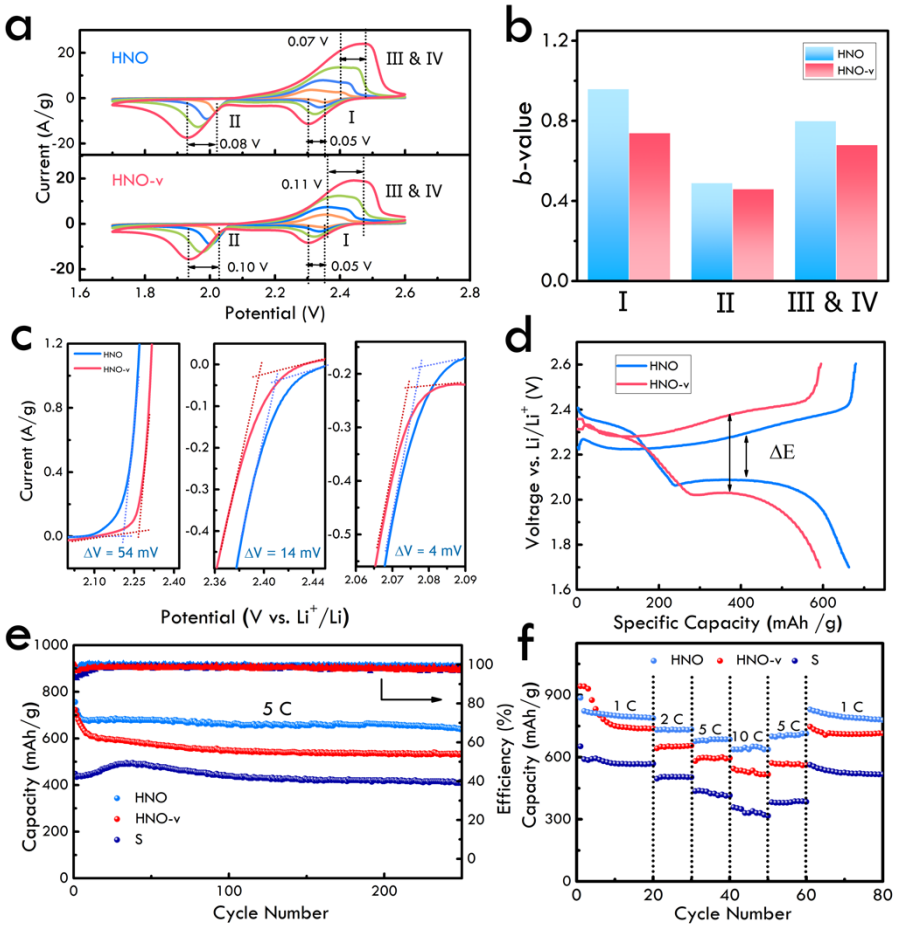

Figure 2. (a) CV curves of HNO and HNO-v cathode with increase scan rate from 0.2 to 2.0 mV/s. The orange, blue, green and red line represents the scan rate of 0.2, 0.5, 1.0 and 2.0 mV/s, respectively. (b) The *b*-values of HNO and HNO-v cathode at the peak I, peak II and peaks III&IV. (c) LSV curves of HNO and HNO-v cathode. (d) Charge/discharge curves and (e) Cycle performance of the HNO, HNO-v, S cathodes at 5 C. (f) Rate capability at different rates of HNO, HNO-v and S cathodes.

Figure 2f shows a comparison between the rate performance of HNO, HNO-v, and a pure sulfur electrode at various currents from 1C to 10C. The reversible capacities of the HNO electrode are 790, 731 and 686 mA h/g at 1C, 2C and 5C. At a large current density of up to 10C, the HNO cathode still achieves a capacity of 637 mA h/g, which is the top among current reports (Table S1). However, the HNO-v can only reach 516 mA h/g at a current density of 10C. When the current returns to 1C, the discharge capacity of HNO will recover to 782 mA h/g, implying an exceptional tolerance in varied current density for broadening applications. It should be noted that the performance difference between HNO and HNO-v became larger with increasing current density. The average capacity difference at 1, 2, 5, 10C are 52.0, 81.7, 90.9, and 125.1 mAh/g. The progressively increasing capacity difference indicated that HNO would be an excellent candidate for high power output Li-S battery without losing much energy density.

In order to elucidate the reason for the better kinetics of HNO, we firstly took X-ray photoelectron spectroscopy (XPS) to study the valence state of both samples. The oxidation states of niobium element in HNO and HNO-v were shown in Figure 3a and 3b. In the Nb 3d spectrum, the Nb $3d_{5/2}$ and Nb $3d_{3/2}$ doublet peaks around 206.8 and 209.6 eV were found in the HNO sample, which refers to two peaks for Nb^{5+}. In contrast, the HNO-v sample showed additional peaks at 210.8 and 207.2 eV, which are be attributed to the increasing concentration of Nb^{4+}.[9b, 11] This observation strongly supports that the HNO-v sample possesses remarkably richer oxygen vacancies. It can also be seen from the XPS signal of oxygen that the adsorption oxygen species significantly increased enhances by introducing vacancies (Figure 3c). The peaks at 529.7 eV arose from the lattice oxygen, while the peaks at 531.4 eV originated from the surface adsorbed oxygen or oxygen vacancies.[12] Moreover, the introduction of these surface defects will largely hinder the electrical conductivity as shown in Figure 3d and Figure S12. The electrical conductivity of HNO is two orders of magnitudes higher than HNO-v, which support that the fully oxidized sample is a better electronic conductor outperformed the HNO-v electrode. The lower conductivity would hinder the electron transport and therefore the polysulfide conversion process would be slowed down due to the sluggish charge compensation.

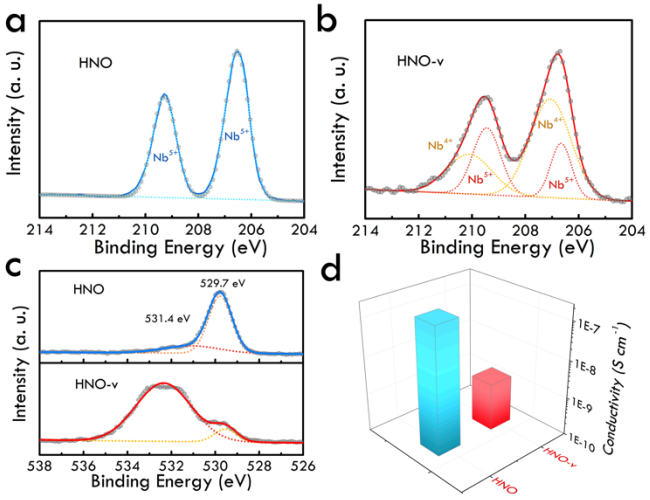

Figure 3. XPS spectra of Nb3d peaks performed on (a) HNO nanobelt and (b) HNO-v. (c) XPS spectra of O1s performed on HNO and HNO-v. (d) Electric conductivities of HNO and HNO-v.

Besides lower conductivity hindered the polysulfide conversion, theoretical studies also showed that adsorption behaviors of polysulfides are quite different between two catalysts. We investigated the adsorption behaviors of reaction mediates lithium polysulfides (Li_2S_4 and Li_2S_6) on both surfaces of HNO and HNO-v. The structure of Li_2S_4 and Li_2S_6 have been constructed and relaxed (Figure 4a), which is consistent with previous references.[6b] The projected density of states (PDOSs) identified that Nb-4d and O-2p_σ have a well-matched covering range, which indicates a stable bonding system (Figure 4b). The S-3p_π orbitals are predominantly localized near E_F. The dominant peak of Li_2S_4 is located at Fermi level (E_F = 0 eV) while that of Li_2S_6 occupies 1.0 eV below E_F. Meanwhile, the O-2p_π orbitals and S-3p_π orbitals are well overlapped. To further investigate the adsorption behaviors, we carefully compare the electronic structures between the pristine and O-deficit surfaces (Figure 4c and 4d). The dominant S-3p_π orbitals in lithium polysulfides shift towards a lower position, which has evidently reduced the gap with O-2p_π. This reduced gap will induce the stronger repulsion between the lone pair of electrons. Particularly, the O-2p_π orbitals and S-3p_π orbitals are well matched in the adsorption of Li_2S_6 in the O-deficit surface, in which the peak distance is only a quarter of that in the pristine surface. This strong overlap substantially exhibits the p-p repulsion, which enhances the adsorption barrier. The inhomogeneous charge distribution near the HNb_3O_8 surface can be attributed to the short-range disorder that lacks Van Hoff singularities. Moreover, the distance between Nb-4d with O-2p_π and S-3p_π orbitals decreases as the appearance of oxygen vacancy as well.

Associated with the electronic structure analysis, we also examine the adsorption behaviors from both the structural and energetic views. After the relaxation, we notice that the protons would migrate from their original positions on the (020) surface of HNb_3O_8, leaving unsaturated oxygen atoms exposed (Figure 4e). The difference of the adsorption behaviors between the pristine and O-deficit surfaces can be visualized by the relaxed structural configurations. Both adsorbates Li_2S_4 and Li_2S_6 experience stronger structural distortion, in which the S atoms are strongly binding with the surface (Figure 4f and 4g). Meanwhile, the structures of Li_2S_4 and Li_2S_6 are basically unchanged on the O-deficit surface. Moreover, in both surfaces, the electron-rich S atoms also display bonding with the nearby protons that causes local unsaturated oxygen atoms. The shortest Li-O distance of Li_2S_4 and Li_2S_6 on the pristine surface is 1.625 Å and 1.540 Å, respectively. In comparison, such distances have increased 1.655 Å and 1.682 Å in the O-deficit surface, which indicate a stronger weaker binding. Therefore, the lower stronger adsorption on the pristine surface can be attributed to the stronger local distortion that can overcome the repulsion barrier induced between O-2p_π and S-3p_π. On the O-deficit surface, the local unsaturated environment will induce the inhomogeneous charge distribution due to the enlarged degree of disorder near the defect. The unsaturation level of the surface O atoms is more evident than the local Nb atoms, which causes stronger local repulsion to the S-2p orbitals from the adsorbates. The calculations of adsorption energies are in good agreement with the results of electronic structures and structural configurations. The adsorption energies of Li_2S_4 and Li_2S_6 on the pristine surface are 1.21 and -0.68 eV, respectively (Figure 4h). The lower adsorption of Li_2S_6 energies can be ascribed to the larger contact surface of the Li_2S_6 with the surface. The adsorption energies of Li_2S_4 have increased nearly nine times on the O-deficit surface to 10.52 eV, representing a very weak bonding. The ΔE_{ads} of Li_2S_6 also obviously increases 4.78 eV that changed from spontaneous adsorption to adsorption with an evident barrier. Therefore, the theoretical results demonstrate the stronger binding strength with pristine HNb_3O_8 surface than the O-deficit surface, which implies that a proper surface modulation with appropriate p-p repulsion are pivotal for restricting the polysulfide shuttling effect in HNb_3O_8.

By combining the above experimental and theoretical results, it can be concluded that oxygen vacancy is not a panacea for all kinds of Li-S battery. Despite the previous investigation on the catalytic role of oxygen vacancies on polysulfides conversion, in the case of niobic acid, too much oxygen vacancies would possibly lead to inferior Li-S battery performance. Therefore, we suggest that the researchers in Li-S battery should pay special attention to vacancy engineering in that the vacancies might play a very complex role in catalytic conversion of polysulfides.

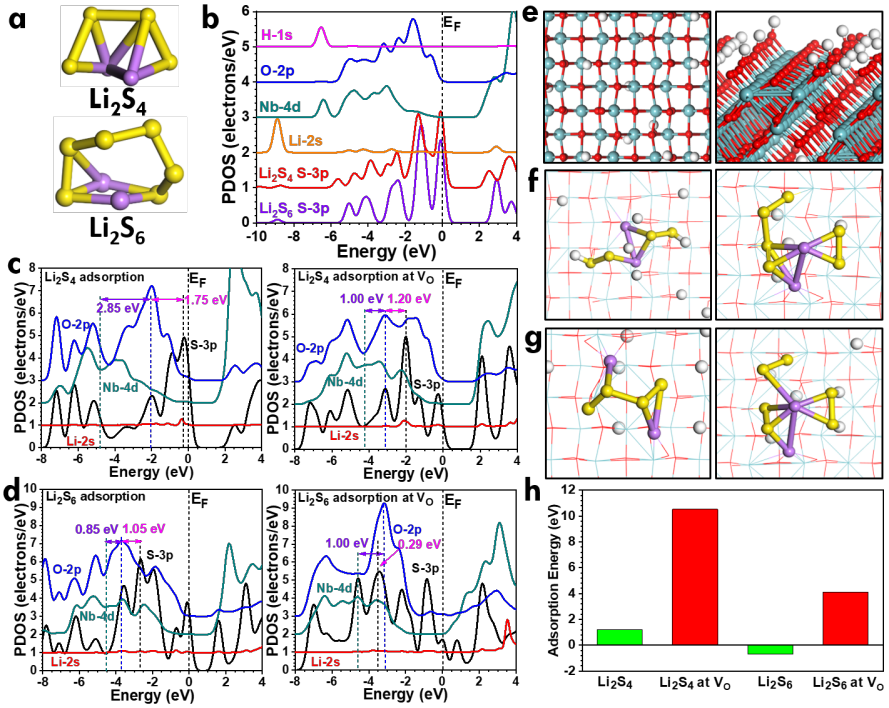

Figure 4. (a) Structure of Li_2S_4 and Li_2S_6. (b) The PDOSs of HNb_3O_8. (c) The PDOSs comparison of Li_2S_4 on pristine and O-deficit HNb_3O_8 (020) surface. (d) The PDOS comparison of Li_2S_6 on pristine and O-deficit surfaces HNb_3O_8 (020) surface. (e) The top view and side view of the relaxed lattice structure of HNb_3O_8 (020) surface. (f) The adsorption behaviors of Li_2S_4 and Li_2S_6 on the pristine surface. (g) The adsorption behaviors of Li_2S_6 on the O-deficit surfaces. (h) The adsorption energies of Li_2S_4 and Li_2S_6 on pristine and O-deficit surfaces. Cyan balls = Nb; Red balls = O; White balls = H, Purple balls = Li and Yellow balls = S.

Conclusion

In summary, the Lewis solid acid HNO and oxygen vacancies rich HNO-v have been investigated as the cathode for Li-S batteries. Unlike many cases, we found the oxygen vacancies on ultrathin niobic acid nanosheets lead to the inferior performance of Li-S batteries. The decrease in performance was mainly attributed to two aspects: Firstly, high oxygen vacancy concentration decreased the electric conductivity. Secondly, O-deficient surface weakened the adsorption of polysulfides. This study showed the paradoxical role of oxygen vacancies in the HNO electrode degraded the electrochemical performance, which is a meaningful reference for vacancy engineering in Li-S battery research.

Acknowledgements

Research reported in this publication was supported by the China National Funds for Excellent Young Scientists (grant no. 21522106), the National Key R&D Program of China (2017YFA0208000) and the National Nature Science Foundation of China (21771156) and the Early Career Scheme (ECS) fund (Grant No.: PolyU 253026/16P) from the Research Grant Council (RGC) of Hong Kong. We thank the Instrument Analysis Center of Xi'an Jiaotong University for their assistance on characterizations.

Keywords: niobic acid • oxygen vacancy • electrochemistry • catalytic conversion • Li-S battery

[1] a) A. Manthiram, Y. Fu, Y.-S. Su, *Acc. Chem. Res.* **2012**, *46*, 1125-1134; b) Y. Yang, G. Zheng, Y. Cui, *Chem. Soc. Rev.* **2013**, *42*, 3018-3032; c) A. Manthiram, Y. Fu, S. H. Chung, C. Zu, Y. S. Su, *Chem. Rev.* **2014**, *114*, 11751-11787; d) K. Xie, Y. You, K. Yuan, W. Lu, K. Zhang, F. Xu, M. Ye, S. Ke, C. Shen, X. Zeng, X. Fan, B. Wei, *Adv. Mater.* **2017**, *29*; e) X. Ji, K. T. Lee, L. F. Nazar, *Nat. Mater.* **2009**, *8*, 500-506.
[2] a) X. Zhu, W. Zhao, Y. Song, Q. Li, F. Ding, J. Sun, L. Zhang, Z. Liu, *Adv. Energy Mater.* **2018**, *8*, 1800201; b) L. Zhang, Z. Chen, N. Dongfang, M. Li, C. Diao, Q. Wu, X. Chi, P. Jiang, Z. Zhao, L. Dong, R. Che, K. P. Loh, H. Lu, *Adv. Energy Mater.* **2018**, *8*, 1802431; c) Y. Yao, W. Feng, M. Chen, X. Zhong, X. Wu, H. Zhang, Y. Yu, *Small* **2018**, *14*, e1802516; d) Q. Pang, X. Liang, C. Y. Kwok, L. F. Nazar, *Nat. Energy* **2016**, *1*.
[3] a) Z. Du, X. Chen, W. Hu, C. Chuang, S. Xie, A. Hu, W. Yan, X. Kong, X. Wu, H. Ji, L. J. Wan, *J. Am. Chem. Soc.* **2019**, *141*, 3977-3985; b) Y. Tao, Y. Wei, Y. Liu, J. Wang, W. Qiao, L. Ling, D. Long, *Energy Environ. Sci.* **2016**, *9*, 3230-3239; c) K. Xi, D. He, C. Harris, Y. Wang, C. Lai, H. Li, P. R. Coxon, S. Ding, C. Wang, R. V. Kumar, *Adv. Sci.* **2019**, *6*, 1800815.
[4] S. Shen, X. Xia, Y. Zhong, S. Deng, D. Xie, B. Liu, Y. Zhang, G. Pan, X. Wang, J. Tu, *Adv. Mater.* **2019**, *31*, e1900009.
[5] a) W. Wu, J. Pu, J. Wang, Z. Shen, H. Tang, Z. Deng, X. Tao, F. Pan, H. Zhang, *Adv. Energy Mater.* **2018**, *8*, 1702373; b) X. Liang, Y. Rangom, C. Y. Kwok, Q. Pang, L. F. Nazar, *Adv. Mater.* **2017**, *29*; c) J. Zheng, J. Tian, D. Wu, M. Gu, W. Xu, C. Wang, F. Gao, M. H. Engelhard, J. G. Zhang, J. Liu, J. Xiao, *Nano Lett.* **2014**, *14*, 2345-2352; d) J.-J. Chen, R.-M. Yuan, J.-M. Feng, Q. Zhang, J.-X. Huang, G. Fu, M.-S. Zheng, B. Ren, Q.-F. Dong, *Chem. Mater.* **2015**, *27*, 2048-2055.

[6] a）Z. Hao, R. Zeng, L. Yuan, Q. Bing, J. Liu, J. Xiang, Y. Huang, *Nano Energy* **2017**, *40*, 360-368; b）L. Kong, X. Chen, B. Q. Li, H. J. Peng, J. Q. Huang, J. Xie, Q. Zhang, *Adv. Mater.* **2018**, *30*; c）H. Lin, S. Zhang, T. Zhang, H. Ye, Q. Yao, G. W. Zheng, J. Y. Lee, *Adv. Energy Mater.* **2018**, *8*, 1801868; d）X. Liu, J. Q. Huang, Q. Zhang, L. Mai, *Adv. Mater.* **2017**, *29*; e）Z. Z. Yang, H. Y. Wang, L. Lu, C. Wang, X. B. Zhong, J. G. Wang, Q. C. Jiang, *Sci. Rep.* **2016**, *6*, 22990; f）H. C. Wang, C. Y. Fan, Y. P. Zheng, X. H. Zhang, W. H. Li, S. Y. Liu, H. Z. Sun, J. P. Zhang, L. N. Sun, X. L. Wu, *Chem. Eur. J.* **2017**, *23*, 9666-9673; g）H. Wei, E. F. Rodriguez, A. S. Best, A. F. Hollenkamp, D. Chen, R. A. Caruso, *Adv. Energy Mater.* **2017**, *7*, 1601616; h）D. Luo, G. Li, Y. P. Deng, Z. Zhang, J. Li, R. Liang, M. Li, Y. Jiang, W. Zhang, Y. Liu, W. Lei, A. Yu, Z. Chen, *Adv. Energy Mater.* **2019**, *9*, 1900228; i）Y. Wang, R. Zhang, J. Chen, H. Wu, S. Lu, K. Wang, H. Li, C. J. Harris, K. Xi, R. V. Kumar, S. Ding, *Adv. Energy Mater.* **2019**, 1900953.
[7] S. B. Patil, H. J. Kim, H.-K. Lim, S. M. Oh, J. Kim, J. Shin, H. Kim, J. W. Choi, S.-J. Hwang, *ACS Energy Lett.* **2018**, *3*, 412-419.
[8] W. Yang, J. Xiao, Y. Ma, S. Cui, P. Zhang, P. Zhai, L. Meng, X. Wang, Y. Wei, Z. Du, B. Li, Z. Sun, S. Yang, Q. Zhang, Y. Gong, *Adv. Energy Mater.* **2019**, *9*, 1803137.
[9] a）S. Liang, L. Wen, S. Lin, J. Bi, P. Feng, X. Fu, L. Wu, *Angew. Chem. Int. Ed.* **2014**, *53*, 2951-2955; b）J. Xiong, L. Wen, F. Jiang, Y. Liu, S. Liang, L. Wu, *J. Mater. Chem. A* **2015**, *3*, 20627-20632; c）H. Liu, H. Zhang, P. Shen, F. Chen, S. Zhang, *Langmuir* **2016**, *32*, 254-264; d）A. Takagaki, M. Sugisawa, D. Lu, J. N. Kondo, M. Hara, K. Domen, S. Hayashi, *J. Am. Chem. Soc.* **2003**, *125*, 5479-5485.
[10] W. G. Lim, C. Jo, A. Cho, J. Hwang, S. Kim, J. W. Han, J. Lee, *Adv. Mater.* **2019**, *31*, e1806547.
[11] a）J. Chen, H. Wang, Z. Zhang, L. Han, Y. Zhang, F. Gong, K. Xie, L. Xu, W. Song, S. Wu, *J. Mater. Chem. A* **2019**, *7*, 5493-5503; b）S. Li, C. N. Schmidt, Q. Xu, X. Cao, G. Cao, *ChemNanoMat* **2016**, *2*, 675-680.
[12] M. Li, X. He, Y. Zeng, M. Chen, Z. Zhang, H. Yang, P. Fang, X. Lu, Y. Tong, *Chem. Sci.* **2015**, *6*, 6799-6805.

Entry for the Table of Contents (Please choose one layout)

RESEARCH ARTICLE

Text for Table of Contents

Rich oxygen vacancies on ultrathin niobic acid nanosheets will lead to inferior performance of Li-S battery.

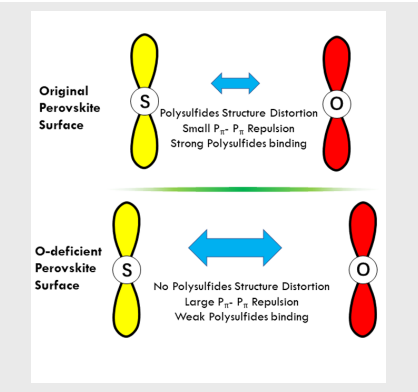

Lingling Xu, Hongyang Zhao, Bolong Huang, Jianwei Wang, Jiale Xia, Na Li, Dandan Yin, Meng Luo, Feng Luo, Yaping Du,* and Chunhua Yan*

Page No. – Page No.

Oxygen Vacancies on Layered Niobic Acid Weaken the Catalytic Conversion of Polysulfides in Lithium Sulfur Battery